HHS Public Access

Author manuscript

Dev Cell. Author manuscript; available in PMC 2018 June 05.

Published in final edited form as:

Dev Cell. 2017 June 05; 41(5): 467–480.e3. doi:10.1016/j.devcel.2017.05.005.

Endothelial-to-osteoblast conversion generates osteoblastic metastasis of prostate cancer

Song-Chang Lin[1,*], **Yu-Chen Lee**[1,*], **Guoyu Yu**[1,*], **Chien-Jui Cheng**[8], **Xin Zhou**[4], **Khoi Chu**[2], **Monzur Murshed**[6], **Nhat-Tu Le**[3], **Laura Baseler**[5], **Jun-ichi Abe**[3], **Keigi Fujiwara**[3], **Benoit deCrombrugghe**[4], **Christopher J. Logothetis**[2], **Gary E. Gallick**[2], **Li-Yuan Yu-Lee**[7], **Sankar N. Maity**[2], and **Sue-Hwa Lin**[1,2,9,#]

[1]Departments of Translational Molecular Pathology, The University of Texas M. D. Anderson Cancer Center, Houston, Texas 77030

[2]Department of Genitourinary Medical Oncology, The University of Texas M. D. Anderson Cancer Center, Houston, Texas 77030

[3]Department of Cardiology, The University of Texas M. D. Anderson Cancer Center, Houston, Texas 77030

[4]Department of Genetics, The University of Texas M. D. Anderson Cancer Center, Houston, Texas 77030

[5]Department of Veterinary Medicine and Surgery, The University of Texas M. D. Anderson Cancer Center, Houston, Texas 77030

[6]Department of Medicine, McGill University, Montreal, QC, Canada

[7]Department of Medicine, Baylor College of Medicine, Houston, Texas 77030

[8]Department of Pathology, Taipei Medical University and Hospital, Taipei, Taiwan

Summary

Prostate cancer (PCa) bone metastasis is frequently associated with bone-forming lesions, but the source of the osteoblastic lesions remains unclear. We show that the tumor-induced bone derives partly from tumor-associated endothelial cells that have undergone endothelial-to-osteoblast (EC-

[#]Correspondence: slin@mdanderson.org (S.-H. L).
[9]Lead Contact
[*]Equal contribution

Disclosure of Potential Conflicts of Interest

C. Logothetis reports receiving a commercial research grant from Astellas, BMS, Sanofi, Janssen, Bayer, and Medivation; has received speakers bureau honoraria from Astellas, Janssen, Sanofi, and Bayer; and is a consultant/advisory board member for Astellas, Janssen, Sanofi, and Bayer. No potential conflicts of interest were disclosed by the other authors.

Author Contributions

Conceptualization, S.-H. L., S.N.M., B.D., G.E.G., and L.-Y.Y.-L.; Methodology, S.-C.L., Y.-C.L., G.Y., X.Z., K.C., M.M., and N.-T.L.; Investigation, S.-H.L., S.-C.L., Y.-C.L., G.Y., X.Z. L.B., and N.-T.L.; Data Analysis and Interpretation, S.-H.L., S.N.M., S.-C.L., Y.-C.L, G.Y., G.E.G., X.Z., C.-J.C., L.B., and L.-Y.Y.-L.; Writing, Review and Editing, S.-H.L., S.N.M., L.-Y.Y.-L., G.E.G., S.-C.L., C..J.L., J.-I.A., L.B., and K.F.; Funding Acquisition, S.-H.L.; Resources, B.D., X.Z. J.-I.A., K.F., and C.J.L.; Supervision, S.-H.L.

to-OSB) conversion. The tumor-associated osteoblasts in PCa bone metastasis specimens and patient-derived xenografts (PDX) were found to co-express endothelial marker Tie-2. BMP4, identified in PDX conditioned media, promoted EC-to-OSB conversion of 2H11 endothelial cells. BMP4-overexpression in non-osteogenic C4-2b PCa cells led to ectopic bone formation under subcutaneous implantation. Tumor-induced bone was reduced in trigenic mice (*Tie2*^{cre}/*Osx*$^{f/f}$/*SCID*) with endothelial-specific deletion of osteoblast cell-fate determinant OSX versus in bigenic mice (*Osx*$^{f/f}$/*SCID*). Thus, tumor-induced EC-to-OSB conversion is one mechanism that leads to osteoblastic bone metastasis of PCa.

Blurb

Lin et al. show that osteoblasts in prostate cancer bone metastasis specimens co-express osteoblast and endothelial markers. Prostate cancer cell-secreted BMP4 converts tumor-associated endothelial cells into osteoblasts in the bone marrow. This endothelial-to-osteoblast conversion is one mechanism underlying the bone-forming lesions of prostate cancer bone metastasis.

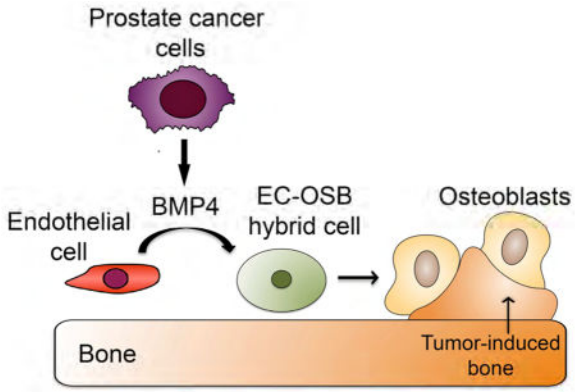

Keywords

prostate cancer; bone metastasis; osteoblast; proteomics; paracrine factors; endothelial-to-osteoblast conversion

Introduction

A distinct feature of human prostate cancer (PCa) is the propensity to metastasize to bone and the generation of osteoblastic bone lesions (Logothetis and Lin, 2005). Clinically, bone metastasis from PCa causes pain, compression of the spinal cord, bone fracture, ineffective hematopoiesis, and death (Coleman, 1997). Several studies have shown that PCa-induced osteogenesis promotes tumor growth (Chen et al., 2007; Gordon et al., 2009; Jacob et al., 1999; Khodavirdi et al., 2006; Lee et al., 2011). The recent success of the bone-targeting radionuclide Radium-223 in the treatment of PCa bone metastasis further supports a role of tumor-induced bone in PCa progression (Sartor et al., 2014). Thus, interfering with cancer-induced bone formation is one of the newer treatment strategies for PCa bone metastasis.

Cancer-induced bone lesions are generally attributed to the imbalance between bone-forming osteoblasts and bone-degrading osteoclasts. Indeed, the osteoblastic bone lesions of

PCa contain an increased number of “activated osteoblasts” in the tumor-infiltrated bone (Vakar-Lopez et al., 2004). Because osteoblast precursors are present in the bone marrow, it has been generally assumed that the PCa-induced bone results from the activation of nearby, preexisting osteoblast precursors. However, histological assessment of osteoblastic metastases of PCa by Roudier et al. (Roudier et al., 2008) found that early new bone formation did not occur from the adjacent bone surface, but rather was observed in the tumor stroma. The stroma was found to contain spindle-shaped cells that produced osteoid directly in the vascularized connective tissue within the tumor. These observations suggest that PCa-induced new bone may be derived from distinct stromal components.

Tumor-induced angiogenesis, in which endothelial cells are recruited into the tumor, has been shown to be required for tumor growth (Folkman, 1971). Endothelial cells are found to exhibit remarkable plasticity and can be converted to multiple cell types (van Meeteren and ten Dijke, 2012). Endothelial-to-mesenchymal transition (EndMT) has been reported in cardiac fibrosis (Zeisberg et al., 2007a), during which endothelial cells are converted into fibroblasts. A recent report by Medici et al. (Medici et al., 2010) showed that in the mouse Fibrodysplasia Ossificans Progressiva (FOP) model, in which the activated mutant ALK2 kinase is constitutively expressed, the endothelial cells were converted into osteoblasts that formed heterotopic bone. These observations raise the possibility that endothelial cells may be recruited by metastatic prostate tumors to become osteoblasts.

The patient-derived xenograft MDA-PCa-118b (PCa-118b), generated from an osteoblastic bone biopsy, is one of a few PCa xenografts that possess osteogenic potential (Li et al., 2008). PCa-118b not only can induce bone formation when implanted into mouse femur but also can induce ectopic bone formation when inoculated subcutaneously (Lee et al., 2011; Li et al., 2008). As osteoblasts are not normally present at the subcutaneous site, these observations, together with those from Roudier et al. (Roudier et al., 2008), raise the question concerning the origin of cells that are converted to osteoblasts in PCa bone metastasis.

In this study, we show that endothelial cells in the prostate tumor can be converted into osteoblasts by PCa secreted factors and this tumor-induced endothelial-to-osteoblast (EC-to-OSB) conversion may represent one of the mechanisms by which prostate tumors induce osteoblastic bone lesions.

Results

Tumor induces mouse mesenchymal cells to form ectopic bone

Previous studies have shown that implantation of patient-derived xenograft PCa-118b subcutaneously resulted in tumor growth that is accompanied by ectopic bone formation (Lee et al., 2011; Li et al., 2008). Goldner’s Trichome staining further confirmed the presence of mineralized bone in PCa-118b tumor (Figure 1A). In contrast, tumors generated from C4-2b cells (Wu et al., 1998), a LNCaP subline, did not contain mineralized bone (Figure 1A). Bone formation is mainly controlled by osteoblasts, which function in the synthesis and deposition of bone extracellular matrix (Ducy et al., 2000). Because osteoblasts are absent at the subcutaneous injection site, ectopic bone formation observed in

the PCa-118b xenograft might be either from tumor cells (human) that have undergone epithelial-to-mesenchymal transition into osteoblast-like cells (Lin et al., 2001), or from other mechanisms, e.g., recruitment of host (mouse) cells that are then converted into osteoblasts. To identify the origin of the osteoblasts in the PCa-118b tumor, we implanted PCa-118b tumor cells subcutaneously into an osteoblast reporter mouse Col-βgal in SCID background. Col-βgal/SCID mouse was generated by crossing the Col-βgal mouse, containing 2.3 kb α1(I) collagen promoter-driven β-gal reporter (Rossert et al., 1995), with SCID mouse (Figure 1Bi). The 2.3 kb α1(I) collagen promoter was previously shown to be mainly active in pre-osteoblast and osteoblast stages of osteogenesis (Figure 1Bi) (Aubin, 1998; Rossert et al., 1995). The expression of the β-gal gene in newborn Col-β gal/SCID mice was highly tissue specific with highest specific activity detected in the long bone and incisors (Figure 1Bii). Similarly, the expression of β-galactosidase, by staining with X-gal substrate, in a newborn mouse showed strong staining in the bones of the skull, ribs, and hind limbs (Figure 1Bii). In the adult Col-βgal/SCID mice, histological sections showed that the β-galactosidase transgene is expressed in osteoblasts (Figure 1Biii, arrowheads) but not in osteocytes (Figure 1Biii, arrows), consistent with the temporal expression of type I collagen in vivo (Aubin, 1998). These data indicate that the 2.3 kb α1(I) collagen promoter directs osteoblast-specific expression of β-galactosidase protein in the Col-βgal/SCID mice.

When the PCa-118b tumor cells were implanted subcutaneously into Col-βgal/SCID mice, the resulting tumors contained ectopic bone (Figure 1Ci). Upon staining the PCa-118b xenografts for β-gal activity, cells that were positive with β-gal activity were detected within the tumors (Figure 1Cii). Most of the β-gal positive cells were present within the immature collagen matrix (Figure 1Cii), which is indicated by the eosin counter stain that revealed varying degrees of collagen extracellular matrix formation within the tumor (Figure 1Cii). However, in the more mature collagen deposit, as reflected in the intensity of eosin staining, β-gal positive cells were located at the edge of the mature bone matrix (Figure 1Ciii). These observations suggest that the osteoblasts present in the ectopic bone of PCa-118b xenograft are of mouse origin.

To further confirm the mouse origin of the osteoblasts observed in the ectopic bone in PCa-118b xenograft, we performed RT-PCR using mouse or human-specific primers for osteocalcin, a marker for differentiated osteoblasts, using RNAs prepared from whole tumor. We found that messages for mouse osteocalcin were much higher than human osteocalcin in PCa-118b xenograft (Figure 1D). We also compared the expression of human osteocalcin in isolated PCa-118b cells with several PCa cell lines including PC3 cells, which was reported to express osteocalcin (Yeung et al., 2002). Relatively low levels of osteocalcin were detected in isolated PCa-118b cells compared to PC3 cells (Figure 1D). Together, these observations suggest that PCa-118b xenograft tumors recruited host (mouse) cells and converted them into osteoblasts (Figure 1E), however, the involvement of tumor cells cannot be completely excluded.

Osteoblasts in PCa-118b-induced bone express endothelial cell markers

The type of mesenchymal cells that are converted to osteoblasts is not clear. Tumors are known to recruit cells from the host microenvironment to support their growth. One possible

source for the tumor-associated osteoblasts in PCa-118b tumor is endothelial cells. To examine this possibility, we performed immunohistochemical staining for the expression of Tie2, an endothelial cell marker, and osteocalcin, an osteoblast marker, in PCa-118b tumor. As a control, calvarial osteoblasts isolated from newborn mice were found to be positive for osteocalcin but not Tie2 (Figure 2A). In contrast, endothelial cells isolated from mouse lung are positive for Tie2 but not osteocalcin (Figure 2A). Validation of the Tie2 and osteocalin antibodies as well as other antibodies used in this study is shown in Figure S1. We found that in the area that contains tumor-induced bone, the cells that are positive with osteocalcin co-localized with cells that are positive for Tie2, and the osteocalcin-Tie2 double-staining cells were localized at the periphery of the tumor-induced bone (Figure 2B). In contrast, the expression of human EpCAM, an epithelial cell marker, did not co-localize with mouse osteocalcin in tumor-induced bone (Figure 2C). Further, in the area that mainly contained tumor cells, the tumor cells were positive for EpCAM but not osteocalcin staining (Figure 2C). These results show that osteoblasts in PCa-118b-induced bone co-express the endothelial cell marker Tie2.

We further examined the expression of markers in individual cells by separating tumor cells from osteoblasts in the PCa-118b tumor. PCa-118b tumor was first digested with Accumax to obtain the “first cell isolate”. The bone-containing fraction was further digested with collagenase to obtain “second cell isolate” (Figure 2D). Upon immunostaining, cells in the first cell isolate were positive for human EpCAM, while cells in second cell isolate were largely negative for EpCAM, suggesting that the first cell isolate but not second cell isolate is enriched with epithelial cells (Figure 2E). On the other hand, both the first-cell-isolate and second-cell-isolate were found to contain Tie2 positive cells, suggesting the presence of endothelial cells in both fractions (Figure 2F). However, the Tie2 positive cells in the first-cell-isolate were negative for osteocalcin (Figure 2F). In contrast, cells from the second-cell-isolate were positive for both Tie2 and osteocalcin (Figures 2F and S2A). Similar results were obtained when cells were stained for Tie1, another endothelial cell marker (Figure S2B). These observations indicate that cells in the second-cell-isolate are likely in transition from endothelial cells to osteoblasts. Together, these observations suggest that osteoblasts present in PCa-118b tumors are likely derived from endothelial cells, supporting EC-to-OSB conversion.

Osteocalcin-Tie2 double-staining cells in human PCa bone metastasis specimens

To determine whether the observed EC-to-OSB conversion in PCa-118b is clinically relevant, paraffin-embedded human PCa bone metastasis specimens were stained for the expression of osteocalcin and Tie2. We examined 15 specimens from bone marrow biopsies of patients with PCa and bone metastasis; 14 from needle biopsy and one from a laminectomy. Tumor cells were found in 14/15 specimens and osteoblasts were found in all 14 specimens positive for tumor. We detected co-staining of osteocalcin and Tie2 in osteoblasts rimming the bone in the laminectomy and 13 needle biopsy specimens by using both fluorescence and confocal microscopy (Figures 2G, S3, & S4), suggesting that these osteocalcin and Tie2 double-positive cells were undergoing EC-to-OSB conversion. Together, these observations suggest that the type of mouse cell that is converted to an osteoblast is the endothelial cell (Tie-2 positive, osteocalcin negative), which undergoes an

intermediate cell type (Tie-2 positive, osteocalcin positive) before becoming a mature osteoblast (Tie-2 negative, osteocalcin positive) (Figure 2H).

BMP4 but not TGFβ2 induces endothelial-to-osteoblast conversion

It is likely that PCa-118b tumor cells secreted factors that induce endothelial cells to become osteoblasts. Medici et al. (Medici et al., 2010) showed that treatment of human endothelial cells with BMP4 or TGFβ2 caused endothelial-to-mesenchyme transition (EndMT) with an increase in osteogenic potential in endothelial cells. Interestingly, our previous studies using cytokine array (Lee et al., 2011) and mass spectrometry (Lee et al., 2015) analyses identified secreted factors, including BMP4 and TGFβ2, in the conditioned medium of PCa-118b cells. Thus, we examined whether BMP4 or TGFβ2 might be involved in EC-to-OSB conversion in mouse endothelial cells. The endothelial cell line 2H11 (Walter-Yohrling et al., 2004) was treated with BMP4 or TGFβ2 in osteoblast differentiation medium for 7 days. We found that treatment with BMP4 led to a dose-dependent increase in the expression of alkaline phosphatase, a marker of osteoblast differentiation, as measured by an increase in staining (Figure 3A, left panel), total alkaline phosphatase activity (Figure 3A, middle panel), and specific activity of alkaline phosphatase (Figure 3A, right panel). In contrast, TGFβ2 did not exert an effect on alkaline phosphatase (Figure 3A). BMP4 treatment also led to an increase in osteocalcin message levels as determined by qRT-PCR while TGFβ2 did not (Figure 3B, left panel). The level of osteocalcin in BMP4-treated 2H11 cells is comparable with that in primary osteoblasts isolated from mouse calvaria (Figure 3B, right panel). Furthermore, treatment of 2H11 cells with BMP4 in differentiation medium for 21 days led to mineralization as indicated by Alizarin Red (Figure 3C) and von Kossa staining (Figure 3D). These observations suggest that BMP4, but not TGFβ2, has the potential to convert 2H11 endothelial cells towards mature osteoblasts. Western blot analysis showed that the increases in osteoblast differentiation induced by BMP4 were accompanied by an increase in the level of cadherin-11 (also known as osteoblast cadherin, OB-cadherin) (Bourne et al., 2004; Kawaguchi et al., 2001 ; Okazaki et al., 1994), a mesenchymal cadherin (Figure 3E). Interestingly, TGFβ2 slightly induces cadherin-11 (Figure 3E), although it did not induce markers for osteoblast differentiation (Figure 3A–3D). Together, these data suggest that tumor-derived BMP4 is one of the factors that can induce endothelial cells to transition into the osteoblast lineage. These results are consistent with our previous observation that treatment of mice bearing PCa-118b tumors with BMP receptor inhibitor LDN193189 reduced tumor-induced bone formation (Lee et al., 2011).

Expression of BMP4 in C4-2b cells induces ectopic bone formation in vivo

Next, we expressed BMP4 or TGFβ2 in non-osteogenic C4-2b PCa cells and examined whether these factors are able to induce ectopic bone formation in vivo. BMP4 or TGFβ2 was overexpressed in C4-2b cells using a bicistronic retroviral vector. RT-PCR confirmed the expression of the BMP4 and TGFβ2 messages (Figure 3F). Western blot showed the C4-2b-TGFβ2 cells secreted TGFβ2 into the conditioned medium (Figure 3F) and ELISA showed that BMP4 was present in the conditioned medium of C4-2b-BMP4 cells at around 32 ng/ml (Figure 3F). Expression of BMP4 or TGFβ2 in C4-2b cells did not have a significant effect on C4-2b cell proliferation in vitro (Figure S5A). These cells were injected subcutaneously into SCID mice. Upon histological analysis of the tumors with hematoxylin

and eosin staining, marked bone-like structures were observed in C4-2b-BMP4 tumors, but not C4-2b-TGFβ2 tumor (Figure 3G). Goldner's Trichrome stain further confirmed that the bone-like matrix was mineralized (Figures 3G and S5B). The C4-2b-BMP4-induced bone tended to be located close to the periphery of the tumor. Quantification of the bone volume, based on the Goldner's Trichrome staining, showed that the C4-2b-BMP4-induced ectopic bone was around 10% of total tumor volume (Figure 3G). In C4-2b-TGFβ2 tumors, extracellular matrices were found to be abundant, encasing the tumor cells (Figures 3G and S5B). However, the abundant matrix in C4-2b-TGFβ2 tumors did not stain with Goldner's Trichrome stain (Figures 3G and S5B), suggesting that the matrix was not mineralized. In addition, scattered red blood cells were frequently seen in C4-2b-TGFβ2 tumors (Figures 3G, arrows, and S5B), suggesting an abnormality in vessel integrity. No significant extracellular matrix or bone-like structures were seen in control C4-2b-vector tumors (Figures 3G and S5B). To further show that C4-2b-BMP4-induced bone is mineralized, von Kossa stain was performed on non-decalcified C4-2b tumors. As shown in Figures 3H and S5C, positive von Kossa staining (black) was observed in C4-2b-BMP4 tumors, but not in C4-2b-TGFβ2 or C4-2b-vector tumors. Osteoid (uncalcified bone matrix) was frequently seen adjacent to calcified bone matrix in C4-2b-BMP4 tumors (Figures 3H and S5C), indicating new bone formation. These observations suggest that tumor-secreted BMP4, but not TGFβ2, plays a role in inducing EC-to-OSB conversion to form ectopic bone.

Human prostate cancer cells in bone metastases express high levels of BMP4

To address whether the findings are clinically relevant, we examined the expression of BMP4 in human prostate cancer specimens from primary prostate cancer and bone metastases by immunohistochemistry. We found that BMP4 expression was low in 15 primary tumors (Figures 3I and S5D) and focally positive (less than 5%) in one specimen. In contrast, BMP4 was highly expressed in 10 of 12 needle biopsy specimens from bone metastasis that contained tumor cells (Figures 3I and S5D). The staining for BMP4 in the other two bone metastasis specimens was medium and weak, respectively (Figure S5D). BMP4 protein was localized in the cytoplasm or the adjacent extracellular space (Figures 3I and S5D), consistent with its role as a secretory protein. The differences in BMP4 expression between bone metastasis and primary tumors are significant ($p=0.00003$) when the BMP4 staining intensity was quantified by Aperio ImageScope software. These observations suggest that BMP4 is expressed in a significant fraction of metastatic prostate cancer cells in bone and likely plays a role in the generation of osteoblastic bone metastasis through inducing EC-to-OSB conversion (Figure 3J).

We also examined the expression of TGFβ2 in several human PCa specimens. We found that TGFβ2 was heterogeneously expressed in primary tumors (Figure S5E). In bone metastasis specimens, TGFβ2 was highly expressed (Figure S5E). These observations were consistent with PCa-118b, which was derived from bone metastasis specimens and expressed both BMP4 and TGFβ2.

Co-localization of osteocalcin and tdTomato in osteoblasts of tumor-induced bone in $Tie2^{Cre}/Rosa^{tdTomato}$ mouse

Lineage tracing with labeled endothelial cells in vivo is an additional method to show that tumor-induced osteoblasts are from endothelial cells. Because implanting PCa-118 cells would require mice in a SCID background (Scid/Scid), which is time consuming, we implanted syngeneic prostate cancer cell line (Tramp-C2) from TRAMP mice (Foster et al., 1997) to overcome the requirement of a SCID background. To promote the cells to induce osteoblastic bone lesions, we overexpressed BMP4 in the Tramp-C2 cell line (Tramp-BMP4). We found that injection of Tramp-BMP4 cells intrafemorally into a male $Tie2^{Cre}/Rosa^{tdTomato}$ mouse generated osteoblastic bone lesion that could be detected by X-ray and μCT (Figure 4A). Upon histological analysis, we observed tumor-induced bone formation and cells with red fluorescence on the surface of the tumor-induced bone (Figure 4B). Immunostaining with anti-osteocalcin antibody showed co-staining of osteocalcin and the tdTomato red fluorescence in osteoblasts rimming the tumor-induced bone (Figures 4C and S6). In the control male $Rosa^{tdTomato}$ mouse without Tie2-Cre, injection of Tramp-BMP4 cells intrafemorally generated bone within the tumor, however, no red fluorescence was detected in the tumor-induced bone (data not shown). These observations are consistent with the notion that osteoblasts in bone metastases are derived from an endothelial (Tie2-expressing) precursor.

Osterix is necessary for osteoblast maturation

Osterix (OSX, Sp7) is a transcription regulator expressed specifically in bone-forming osteoblasts (Nakashima et al., 2002) (Hojo et al., 2016). *Osx*-null mice have a normal cartilagenous skeleton but are completely defective in endochondral and intramembranous bone formation (Nakashima et al., 2002), suggesting that OSX plays a critical role in the development of the osteoblast lineage. To examine the role of OSX in osteoblast differentiation, we isolated calvarial osteoblasts from newborn mice carrying one floxed allele of OSX without ($Osx^{f/+}$) or with ($Osx^{f/-}$) the second allele deleted. To delete the floxed OSX allele from $OSX^{f/+}$ osteoblasts, they were infected with adenovirus containing cre recombinase (Ad-cre) (Figure S7A, left panel). Real-time RT-PCR of the mRNA from these osteoblasts showed that the level of *Osx* message in Ad-cre treated $Osx^{\Delta/-}$ cells is about 2–5% of that in the control $Osx^{\Delta/+}$ cells (Figure S7A, middle panels). Upon culturing in differentiation medium for 14 or 21 days, the message levels of alkaline phosphatase and bone sialoprotein (Bsp) were significantly lower in $Osx^{\Delta/-}$ cells compared to those in $Osx^{\Delta/+}$ cells (Figure S7A, middle panels). These observations suggest that OSX is necessary for osteoblast maturation (Figure S7A, right panel).

Osx is upregulated during EC-to-OSB conversion

We considered the possibility that BMP4 may reprogram the endothelial cells toward the osteoblastic lineage by upregulating Osx expression. To test this, 2H11 endothelial cells were treated with or without BMP4 or TGFβ2 and examined for the expression of OSX. qRT-PCR of the RNA from 2H11 cells showed that BMP4 stimulated the expression of OSX (Figure 5A, left panel). In contrast, TGFβ2 did not (Figure 5A, left panel). Western blot further confirm that BMP4 induced the expression of OSX protein with an apparent

molecular mass of 50 kDa in SDS-PAGE (Figure 5A, right panels). These results suggest that BMP4-induced OSX expression may play a role in EC-to-OSB conversion.

To examine whether OSX is necessary for EC-to-OSB conversion, we generated 2H11 cells with knockdown of OSX (2H11-shOSX#1 and 2H11-shOSX#5) (Figure 5B, left panel) and examined their responses to BMP4 treatment. We found that knockdown of OSX in 2H11 cells significantly decreased BMP4-induced osteocalcin expression in both message and protein levels (Figure 5B, middle and right panels). These results suggest that OSX is necessary for BMP4-induced EC-to-OSB conversion.

Next, we examined whether expression of OSX alone is sufficient to induce EC-to-OSB conversion. OSX was overexpressed in 2H11 cells using a bicistronic retroviral vector that contains GFP as a reporter. 2H11 cells transfected with empty GFP vector were used as a control. Real-time RT-PCR showed an increase in OSX mRNA in 2H11-OSX cells compared to the 2H11-GFP control cells (Figure 5Ci). qRT-PCR for the expression of osteocalcin, an OSX target gene, showed only a moderate increase in osteocalcin in 2H11-OSX cells compared to 2H11-GFP control cells (Figure 5Cii, upper panel). However, upon incubation in differentiation medium with BMP4 for 7 days, there was a significant difference in the osteocalcin levels between 2H11-OSX and 2H11-GFP cells (Figure 5Cii, lower panel). Similarly, overexpression of OSX led to a modest but significant increase in alkaline phosphatase activity in 2H11-OSX cells compared to 2H11-GFP cells (Figure 5Ciii, upper panel), with the difference more obvious upon BMP4 treatment (Figure 5Ciii, lower panel). These results suggest that OSX alone is not sufficient to induce EC-to-OSB conversion of 2H11 cells, similar to the work of Zhu et al.(Zhu et al., 2012) that demonstrated OSX is necessary but not sufficient to differentiate human mesenchymal stem cells into osteoblasts. Together, these results suggest that both BMP4 and OSX are required for EC-to-OSB conversion of 2H11 endothelial cells (Figure 5D).

In the report by Medici et al. (Medici et al., 2010) they showed that endothelial cells possess a multipotent stem cell-like property and could be triggered to differentiate into osteoblasts, chondrocytes and adipocytes when treated with BMP4 or TGFβ2. It would be of interest to examine whether BMP4-treated 2H11 cells could be differentiated into adipocyte or chondrocyte lineage cells in addition to osteoblasts. We found that BMP4-treated 2H11 cells could not be induced to form adipocytes, while the pluripotent C3H10T1/2 cells could, as detected by oil red O staining (Figure S7B). Similarly, BMP4-treated 2H11 cells could not be induced to form chondrocytes, while C3H10T1/2 cells could, as detected by Alcian blue staining (Figure S7B). We also examined the changes of molecular markers, including markers of OSB lineage (OSX, Cad11, Col1α1), endothelial lineage (Tie2, VE-Cad), and fibroblast lineage (FSP1, N-cadherin, αSMA, and vimentin) in 2H11 cells treated with or without BMP4 or TGFβ2 using Western blot. We found that BMP4, but not TGFβ2, increases the expression of OSX, Cad11, and Col1α1 (Figure S7C). However, we did not detect consistent changes in markers of endothelial lineage or fibroblast lineage (Figure S7C). We also did not detect the expression of cell junction protein ZO-1 in 2H11 cells (data not shown) and treatment of 2H11 cells with or without BMP4 or TGFβ2 did not affect the migration of 2H11 cells (Figure S7D). Thus, tumor-derived 2H11 cells do not possess the multipotent stem cell-like properties seen in normal endothelial cells.

Generation of a genetically engineered trigenic mouse model with endothelial-specific OSX deletion

Next, we examined the role of EC-to-OSB conversion in PCa-induced osteogenesis in vivo. Because OSX is necessary for EC-to-OSB conversion, we generated mice with endothelial-specific deletion of *Osx* by crossing $Osx^{f/f}$ mice with $Tie2\text{-}Cre^{+/-}$ (B6.Cg-Tg(Tek-cre)12Flv/J, JAX mice database). To allow for implanting human PCa cell lines, the mice were further crossed with SCID mice. The mating strategy is illustrated in Figure 6A. All of the mice were on a C57BL/6 background. Mice with the genotype $Osx^{f/f};Scid^{+/+}$ (without Tie2-cre) are referred to as bigenic, while mice with genotype $Tie2\text{-}Cre^{+/-};Osx^{f/f};Scid^{+/+}$ are referred to as trigenic. The tail genotyping results demonstrated that the trigenic mice carried all transgenes, including Tie2-cre, the floxed *Osx* allele, and SCID homozygosity (Figure 6A). To determine the efficiency of *Osx* gene deletion by Tie2-cre, microvascular endothelial cells were isolated from the lungs of bigenic and trigenic mice using CD31 magnetic beads. Real-time PCR of the genomic DNA in these endothelial cells showed the presence of cre in the endothelial cells of trigenic but not bigenic mice, and that the level of *Osx* gene in the trigenic mice is about 10 % of that in bigenic mice (Figure 6A). These results suggest that we have established an endothelial-specific OSX knockout trigenic mouse line.

To examine whether introducing Tie2-Cre to Osx conditional knockout mice has an effect on vascular or skeletal phenotype of the mice, we first performed histopathological analysis on a trigenic and a bigenic mice. No obvious skeletal or vascular abnormalities were observed (Figure S7E). The lymphoid organs exhibited lymphoid atrophy as expected for SCID mice. We observed rectal prolapse, which may be due to increased infection as the mice are in a SCID background, in both bigenic and trigenic mice. The skeletal phenotype was further examined by performing micro-CT on four pairs of age and sex matched bigenic and trigenic mice. We found that there is no significant difference in the bone mineral density between bigenic and trigenic mice (Figure S7E). Upon histomorphometry analyses on age and sex matched littermates, we also did not find significant difference in several parameters, including BV/TV, BS/BV, BS/TV, Tb.Dm, Tb.N, and Tb.Sp between bigenic and trigenic mice (Figure S7E). The vascular phenotype of bigenic and trigenic mice was further examined by Tie2 immunostaining on lung tissue. We found no significant difference in Tie2 staining in lung (Figure S7E). Thus, there is no significant effect of Tie2-Cre:osterix or on basal skeletal and vascular phenotype.

Endothelial-specific *Osx* deletion reduces PCa-induced osteogenesis in vivo

Next, we injected C4-2b-BMP4 cells into trigenic or bigenic mice subcutaneously and compared the ability of C4-2b-BMP4 cells to induce ectopic bone formation. We found a significant decrease in the amount of bone formation, as revealed by Goldner's Trichome staining, when C4-2b-BMP4 cells were grown subcutaneously in trigenic as compared to bigenic mice (Figure 6B). Because C4-2b cells were generated from castrate-resistant LNCaP tumors (Wu et al., 1998), we found that C4-2b-BMP4 cells were also able to form tumors in female trigenic or bigenic mice. There was a decrease in C4-2b-BMP4 tumor bone volume in female trigenic versus bigenic mice, similar to that observed in the male mice (Figure 6C). Although deficient of OSX in endothelial cells reduces ectopic bone formation

by C4-2b-BMP4 cells, these tumors still contain some bone, likely due to insufficient deletion of *Osx* by Tie2-cre or from other cellular sources that may contribute to osteoblast formation.

Finally, we compared the ectopic bone formation of MDA-PCa-118 tumors implanted in trigenic or bigenic mice. The changes in the formation of mineralized bone were examined by Goldner's Trichome staining. We found that there was a significant decrease in the amount of bone formation when MDA-PCa-118b cells were grown subcutaneously in trigenic compared to bigenic mice (Figure 7A–7B). In our previous studies, we showed that PCa-induced bone formation could influence tumor growth (Lee et al., 2011). To examine whether the inhibition of osteoblast formation from endothelial cells had an impact on tumor growth, PCa-118b cells were injected into bigenic and trigenic mice on the same day and the mice were euthanized at the same time point to compare tumor size. We found that the tumor size in trigenic mice was significantly smaller than in bigenic mice (Figure 7C). Together, these results suggest that tumor-induced EC-to-OSB conversion is one of the mechanisms that lead to osteoblastic bone metastasis of PCa.

Discussion

Our studies showed that tumor-induced EC-to-OSB conversion is one mechanism that contributes to the osteoblastic phenotype of prostate cancer bone metastasis. We showed that PCa-118b cells secrete factors, e.g., BMP4, which are able to convert tumor-induced endothelial cells (or other stromal cells) to osteoblasts to form bone, leading to osteoblastic bone lesions (Figure 7D). Furthermore, we detected the presence of endothelial-osteoblast hybrid cells that were Tie2 and osteocalcin double-positive along the surface of newly-formed bone in human PCa bone metastasis specimens. These findings show that EC-to-OSB conversion occurs clinically. Although EC-to-OSB conversion has reportedly been involved in ectopic bone formation in other diseases such as FOP (Medici et al., 2010), this study is the first to link EC-to-OSB conversion to PCa-induced bone formation and the first to demonstrate the roles of OSX and BMP4 in the process.

Vascular endothelial cells have a remarkable plasticity and have been shown to generate other cell types through endothelial-to-mesenchymal transition (EndMT). Such plasticity is required during embryonic development, e.g. in cardiac development (Markwald et al., 1975). Recently, EndMT was found to be involved in pathological processes, including cardiac fibrosis, diabetic nephropathy, cancer, and heterotopic bone formation (for review, see Medici and Kalluri (Medici and Kalluri, 2012)). Here we further show that tumor-induced EC-to-OSB conversion leads to osteoblastic lesions in PCa bone metastasis. Our findings are consistent with the histologic analysis of human PCa bone metastasis by Roudier et al (Roudier et al., 2008), in which they reported that alkaline phosphatase positive spindle-shaped cells produced osteoid directly in vascularized connective tissue that supported the tumor. It is likely that these "spindle-shaped cells" were endothelial cells that had undergone EC-to-OSB conversion.

Interestingly, Klagsbrun's group (Dudley et al., 2008) showed that endothelial cells isolated from prostate tumors from TRAMP mice could be calcified. It is possible that these PCa-

associated endothelial cells had already undergone EC-to-OSB conversion, likely through factors secreted by the prostate tumor. Thus, PCa may induce EC-to-OSB conversion both in the primary tumor and metastatic sites.

Factors that have been shown to stimulate EC-to-OSB conversion include BMP and TGFβ family proteins. Among BMP family proteins, BMP2 and BMP4 have been shown to stimulate EndMT (Ma et al., 2005; McCulley et al., 2008) while BMP7 inhibits EndMT (Zeisberg et al., 2007b). Among the three TGFβ isoforms, TGFβ2 is the major isoform involved in EC-to-OSB conversion (Azhar et al., 2009; Medici et al., 2011; Medici et al., 2010; Romano and Runyan, 2000), suggesting a unique TGFβ2 receptor signal transduction pathway in endothelial cells. Studies by Medici et al. (Medici et al., 2010) showed that both TGFβ2 and BMP4 could induce normal endothelial cells to undergo EndMT, leading to bone formation. In our study, we found that only BMP4, but not by TGFβ2, could induce ectopic bone formation in C4-2b PCa cells. While BMP4 is critical in EC-to-OSB conversion, exogenous overexpression of BMP4 alone in C4-2b tumors did not induce mineralization in vivo as strongly as that seen in PCa-118b tumors, suggesting the contribution of additional as-yet unidentified factors. In the mouse model of FOP generated by expressing constitutively-active ALK2 (caALK2), the presence of inflammatory stimuli was shown to be required for the development of ectopic ossification (Yu et al., 2008). These factors remain to be identified.

Besides EC-to-OSB conversion, other mechanisms may also be involved in the formation of new bone in PCa bone metastasis. One possibility is that pluripotent mesenchymal stem cells (MSC), which have the potential to give rise to multiple cell types, including osteoblasts (Bourne et al., 2004; Buttery et al., 2001), are recruited to the tumor site and then differentiate into osteoblasts. Eghbali-Fatourechi et al. (Eghbali-Fatourechi et al., 2005) reported that osteoblasts are present in the circulation during periods of normal postnatal bone development. Otsuru et al. (Otsuru et al., 2008) further suggested that circulating osteoblasts that originated from bone marrow-derived osteoblast progenitor cells might contribute to ectopic bone formation in mice. Thus, it is also possible that circulating osteoblasts may be recruited to areas with increased bone formation. Recently, Joseph et al. (Joseph et al., 2012) reported that disseminated PCa cells in the bone marrow interact with the hematopoetic stem cells (HSC) or hematopoetic progenitor cells (HPC), and this led HSC or HPC to secrete BMP2 or IL-6 to affect osteoblast or osteoclast differentiation. Thus, PCa cells may affect bone remodeling indirectly through HSC or HPC. Whether these mechanisms are involved in human PCa bone metastasis awaits further confirmation.

In summary, we have identified endothelial-to-osteoblast conversion as one of the mechanisms that confer the osteoblastic phenotype in PCa bone metastasis. Our studies not only revealed mechanistic insights into the unique bone-forming phenotype of PCa bone metastasis but also provide a new direction for developing treatment strategies for PCa bone metastasis.

METHOD DETAILS

Growth and maintenance of PCa-118b tumors

PCa-118b tumors were passaged in SCID mice as follows. The tumor cells in PCa-118b xenograft were isolated by digesting the tumor with Accumax enzyme mixture (eBioscience) and dissociated tumor cells were cultured for 48 h in CnT-52 medium (Millipore), which selectively allows epithelial but not mesenchymal cells to survive in culture (Lee et al., 2015). The PCa-118b cells in culture were then digested with trypsin and injected into male SCID mice subcutaneously at 1 million cells per site.

Generation of Col-Luc mice in SCID background

Transgenic mice harboring luciferase and β-galactosidase transgenes (Col-βgal mice) that were under the control of 2.3 kb segments of the mouse α1(I) collagen promoter were generated as described previously (Rossert et al., 1995). Col-βgal immunodeficient mice were generated by breeding Col-βgal mice to SCID immunodeficient mice (Col-βgal/SCID). Genotyping for the *scid* allele was performed by PCR of mouse tail DNA followed by Alu I digestion (Maruyama et al., 2002; Sealey et al., 2002). Mice with homozygous *scid* alleles (scid/scid) were used in tumor implantation studies. Mice were maintained in pathogen-free conditions at the MD Anderson Cancer Center. All manipulations were approved by the MD Anderson Cancer Center Institutional Animal Care and Use Committee.

β-galactosidase staining

To assess the expression of β-galactosidase activity in 4-day-old transgenic mice, the skin of mice was removed and whole mice were fixed for 30–40 min in 0.1M $NaPO_4$ (pH 7.3), 2% formalin, 0.2% glutaraldehyde, 5 mM EGTA, and 2 mM $MgCl_2$. After washing, mice were stained overnight with X-gal (1 mg/ml) in PBS containing 2 mM $MgCl_2$, 4 mM potassium ferrocyanide, 5 mM potassium ferricyanide, 0.2% NP-40, and 0.1% sodium deoxycholate. After which the mice were washed in PBS and photographed. For PCa-118b tumors implanted in Col-βgal/SCID mice, the tumors were formalin-fixed, X-gal stained, processed in Histoclear and embedded in paraffin. Tumor sections were counter-stained with eosin.

Reverse transcription and quantitative PCR

Total RNA was extracted from cells using Trizol (InVitrogen) and further purified by RNAeasy mini kit plus DNase I treatment (Qiagen). The relative mRNA level for each gene was quantified by real-time RT-PCR with SYBR Green (Applied Biosystems), using *Gapdh* as a control.

Immunostaining and immunohistochemistry

Formalin-fixed and paraffin-embedded (FFPE) PCa-118b sections were dewaxed, rehydrated, and antigen retrieved using Target Retrieval solution (Dako) according to manufacturer's instructions. Sections were blocked in a buffer of 5% normal serum or MOM blocking solution (Vector Lab PK-2200) for mouse primary antibodies, followed by overnight incubation with primary antibody at 4°C. Sections were washed and incubated with Alexa fluor-conjugated secondary antibodies accordingly. Nuclei were counterstained

by DAPI. Goldner's Trichrome staining was performed on rehydrated FFPE sections using aniline blue (Dorn and Hart Microedge Inc). Microscope images were taken on either an Olympus IX71 fluorescence microscope or an Olympus Confocal FV1000 microscope. Large images were scanned and analyzed by Aperio ImageScope software.

Isolation of tumor cells or stromal cells from PCa-118b tumors

PCa-118b tumors were dissected, cut into small pieces, and digested with Accumax (eBioscience), which contains a mixture of proteases including trypsin. The undigested fraction was collected by filtering the mixture through a 100 μm cell strainer. The filtered fraction that contained PCa-118b cells was centrifuged at 400xg and the cells were collected (1st-isolate). The undigested fraction was further digested with collagenase P and trypsin/EDTA, filtered through a 100 μm cell strainer, and centrifuged at 400xg to collect the cells (2nd-isolate).

Cell differentiation assays

2H11 cells were cultured in serum-free DMEM medium for 48 hours followed by treatment of BMP4 or TGFβ2 for 2 to 3 days. For differentiation to osteoblasts, 2H11 cells were cultured in StemPro osteoblast differentiation medium (InVitrogen) for 7 to 21 days. For adipogenic or chondrogenic differentiation, C3H10T1/2 and 2H11 cells were cultured in StemPro adipogenic or chondrogenic differentiation culture medium (InVitrogen) containing the appropriate stimuli to induce lineage-specific differentiation. Oil Red O staining for adipocytes was performed for 30 min on cells grown in adipogenic medium for 10 days. Alcian blue staining for chondrocytes was performed for 30 min on cells cultured in chondrogenic medium for 14 days.

Alkaline phosphatase activity and mineralization assays

For alkaline phosphatase staining, the culture was fixed with 10% formalin for 1 min and incubated with BCIP/NBT at room temperature for 5–10 min. For Alizarin staining, the formalin-fixed cells were covered with freshly prepared Alizarin Red S solution and incubated at room temperature in the dark for 45 min. Von Kossa staining was performed by treating formalin-fixed cells in 5% silver nitrate, placed in a UV crosslinker for 2 cycles, and washed with water.

Generation of C4-2b cell line overexpressing BMP4 or TGFβ2

C4-2b-LT cells were generated by transfecting C4-2b cell with luciferase reporter and red fluorescent protein-Tomato using bicistronic retroviral vector pBMN-luc-tomato as previously described (Huang et al., 2010). C4-2b-LT cells expressing BMP4 or TGFβ2 were generated as follows. To generate C4-2b-BMP4 or C4-2b-TGFβ2 cells, cDNAs encoding human BMP4 or TGFβ2 were inserted into the bicistronic retroviral vector pBMN-I-Neo and C4-2b-LT cells were infected with retroviruses containing BMP4, TGFβ2, or empty vector. The cells were selected by G418.

Knockdown and overexpression of OSX in 2H11 cells

To knockdown OSX in 2H11 cells, shOSX-vector and five shOSX clones in GIPZ lentiviral vector were used. 2H11-shOSX#1 and 2H11-shOSX#5 were used in this study. 2H11 cells overexpressing OSX (2H11-OSX) were generated by infecting 2H11 cells with retroviral particles generated from the plasmids pBMN-OSX-GFP, constructed by inserting cDNA encoding for mouse OSX into pBMN-I-GFP vector. Control cells (2H11-GFP) were generated by infecting cells with the retroviral vector pBMN-I-GFP.

Generation of $Tie2^{Cre}$/Rosa-tdTomato reporter and $Tie2^{cre}/Osx^{f/f}$/SCID mice

TEK-Cre (B6.Cg-Tg12Flv #004128, Jackson laboratory) mice were bred with B6.Cg-*Gt(ROSA)26Sor* (Rosa-tdTomato) mice (#007914 Jackson Laboratory) to create the Tie2-Cre/Rosa-tdTomato mouse. Male mice were used for *in vivo* lineage tracing study. Tumor cells were injected into right femur of the mouse. After five weeks, mice were subjected to radiograph. Femurs were fixed in PFA, decalcified in EDTA, and embedded in OCT for cryosections. Mice with the conditional *osx* allele $osx^{f/f}$ were generated previously (Zhou et al., 2010). To generate $Tie2^{cre}/Osx^{f/f}/SCID$ mice, we crossed $osx^{f/f}$ mice with B6.CB17-$Prkdc^{scid}/SzJ$ SCID mice (#001913, Jackson Laboratory) and TEK-Cre mice. Genotyping for *Tie2-cre* and *SCID* allele was done by PCRs, following the protocols from the Jackson laboratory. Genotyping for conditional *osx* alleles was performed using the forward primer 5’-CTT GGG AAC ACT GAA GCT GT-3’ and the reverse primer 5’-CTG TCT TCA CCT CAA TTC TAT T-3’ in a PCR reaction of 3 minutes at 95°C, 35 cycles of 30 seconds at 94°C, 30 seconds at 58°C, 1 minute at 72°C, and completed with final extension 5 minutes at 72°C. Both male and female mice were used in xenograft studies.

Bone histomorphometry

Femurs were sectioned at 5 μm thickness in a longitudinal plane. The sections were subsequently stained for Von Kossa (silver staining) to visualize mineralization. Measurements were performed in the mid-cancellous region of the distal metaphysis of the femur on 2 sections spaced 75 μm apart. The region of interest extends 1.5 mm proximally from the distal growth plate excluding a 150 μm region adjacent to the cortical bone and growth plate. Referent data, e.g. BV, TV and BS, from the measurements was pooled from both sections. All other indices were derived from these 3 parameters. The rod model was used to calculate the Trabecular Diameter (Tb.Dm), the Trabecular Number (Tb.N) and the Trabecular spacing (Tb.Sp) as the trabecular bone in long bones is more rod-like or cylindrical in shape.

Supplementary Material

Refer to Web version on PubMed Central for supplementary material.

Acknowledgments

This work was supported by grants from the NIH including CA174798, P50 CA140388 and CA16672, the Prostate Cancer Foundation, Cancer Prevention and Research Institute of Texas (CPRIT RP110327, CPRIT RP150179, CPRIT RP150282), and funds from the University Cancer Foundation via the Sister Institute Network Fund at the MD Anderson Cancer Center.

References

Aubin JE. Advances in the osteoblast lineage. Biochem Cell Biol. 1998; 76:899–910. [PubMed: 10392704]

Azhar M, Runyan RB, Gard C, Sanford LP, Miller ML, Andringa A, Pawlowski S, Rajan S, Doetschman T. Ligand-specific function of transforming growth factor beta in epithelial-mesenchymal transition in heart development. Dev Dyn. 2009; 238:431–442. [PubMed: 19161227]

Bourne S, Polak JM, Hughes SP, Buttery LD. Osteogenic differentiation of mouse embryonic stem cells: differential gene expression analysis by cDNA microarray and purification of osteoblasts by cadherin-11 magnetically activated cell sorting. Tissue Eng. 2004; 10:796–806. [PubMed: 15265297]

Buttery LD, Bourne S, Xynos JD, Wood H, Hughes FJ, Hughes SP, Episkopou V, Polak JM. Differentiation of osteoblasts and in vitro bone formation from murine embryonic stem cells. Tissue Eng. 2001; 7:89–99. [PubMed: 11224927]

Chen N, Ye XC, Chu K, Navone NM, Sage EH, Yu-Lee LY, Logothetis CJ, Lin SH. A secreted isoform of ErbB3 promotes osteonectin expression in bone and enhances the invasiveness of prostate cancer cells. Cancer Res. 2007; 67:6544–6548. [PubMed: 17638862]

Coleman RE. Skeletal complications of malignancy. Cancer. 1997; 80:1588–1594. [PubMed: 9362426]

Ducy P, Schinke T, Karsenty G. The osteoblast: a sophisticated fibroblast under central surveillance. Science. 2000; 289:1501–1504. [PubMed: 10968779]

Dudley AC, Khan ZA, Shih SC, Kang SY, Zwaans BM, Bischoff J, Klagsbrun M. Calcification of multipotent prostate tumor endothelium. Cancer Cell. 2008; 14:201–211. [PubMed: 18772110]

Eghbali-Fatourechi GZ, Lamsam J, Fraser D, Nagel D, Riggs BL, Khosla S. Circulating osteoblast-lineage cells in humans. N Engl J Med. 2005; 352:1959–1966. [PubMed: 15888696]

Folkman J. Tumor angiogenesis: therapeutic implications. The New England journal of medicine. 1971; 285:1182–1186. [PubMed: 4938153]

Foster BA, Gingrich JR, Kwon ED, Madias C, Greenberg NM. Characterization of prostatic epithelial cell lines derived from transgenic adenocarcinoma of the mouse prostate (TRAMP) model. Cancer Res. 1997; 57:3325–3330. [PubMed: 9269988]

Gordon JA, Sodek J, Hunter GK, Goldberg HA. Bone sialoprotein stimulates focal adhesion-related signaling pathways: role in migration and survival of breast and prostate cancer cells. J Cell Biochem. 2009; 107:1118–1128. [PubMed: 19492334]

Hojo H, Ohba S, He X, Lai LP, McMahon AP. Sp7/Osterix Is Restricted to Bone-Forming Vertebrates where It Acts as a Dlx Co-factor in Osteoblast Specification. Developmental cell. 2016; 37:238–253. [PubMed: 27134141]

Huang CF, Lira C, Chu K, Bilen MA, Lee YC, Ye X, Kim SM, Ortiz A, Wu FL, Logothetis CJ, et al. Cadherin-11 increases migration and invasion of prostate cancer cells and enhances their interaction with osteoblasts. Cancer Res. 2010; 70:4580–4589. [PubMed: 20484040]

Jacob K, Webber M, Benayahu D, Kleinman HK. Osteonectin promotes prostate cancer cell migration and invasion: a possible mechanism for metastasis to bone. Cancer Res. 1999; 59:4453–4457. [PubMed: 10485497]

Joseph J, Shiozawa Y, Jung Y, Kim JK, Pedersen E, Mishra A, Zalucha JL, Wang J, Keller ET, Pienta KJ, Taichman RS. Disseminated prostate cancer cells can instruct hematopoietic stem and progenitor cells to regulate bone phenotype. Molecular cancer research : MCR. 2012; 10:282–292. [PubMed: 22241219]

Kawaguchi J, Kii I, Sugiyama Y, Takeshita S, Kudo A. The transition of cadherin expression in osteoblast differentiation from mesenchymal cells: consistent expression of cadherin-11 in osteoblast lineage. J Bone Miner Res. 2001; 16:260–269. [PubMed: 11204426]

Khodavirdi AC, Song Z, Yang S, Zhong C, Wang S, Wu H, Pritchard C, Nelson PS, Roy-Burman P. Increased expression of osteopontin contributes to the progression of prostate cancer. Cancer Res. 2006; 66:883–888. [PubMed: 16424021]

Lee YC, Cheng CJ, Bilen MA, Lu JF, Satcher RL, Yu-Lee LY, Gallick GE, Maity SN, Lin SH. BMP4 Promotes Prostate Tumor Growth in Bone through Osteogenesis. Cancer Res. 2011; 71:5194–5203. [PubMed: 21670081]

Lee YC, Gajdosik MS, Josic D, Clifton JG, Logothetis C, Yu-Lee LY, Gallick GE, Maity SN, Lin SH. Secretome Analysis of an Osteogenic Prostate Tumor Identifies Complex Signaling Networks Mediating Cross-talk of Cancer and Stromal Cells Within the Tumor Microenvironment. Molecular & cellular proteomics : MCP. 2015; 14:471–483. [PubMed: 25527621]

Li Z, Mathew P, Yang J, Starbuck MW, Zurita AJ, Liu J, Sikes C, Multani AS, Efstathiou E, Lopez A, et al. Androgen receptor–negative human prostate cancer cells induce osteogenesis through FGF9-mediated mechanisms. J Clin Invest. 2008; 118:2697–2710. [PubMed: 18618013]

Lin DL, Tarnowski CP, Zhang J, Dai J, Rohn E, Patel AH, Morris MD, Keller ET. Bone metastatic LNCaP-derivative C4–2B prostate cancer cell line mineralizes in vitro. Prostate. 2001; 47:212–221. [PubMed: 11351351]

Logothetis C, Lin SH. Osteoblasts in prostate cancer metastasis to bone. Nature Reviews Cancer. 2005; 5:21–28. [PubMed: 15630412]

Ma L, Lu MF, Schwartz RJ, Martin JF. Bmp2 is essential for cardiac cushion epithelial-mesenchymal transition and myocardial patterning. Development. 2005; 132:5601–5611. [PubMed: 16314491]

Markwald RR, Fitzharris TP, Smith WN. Sturctural analysis of endocardial cytodifferentiation. Dev Biol. 1975; 42:160–180. [PubMed: 1112439]

Maruyama C, Suemizu H, Tamamushi S, Kimoto S, Tamaoki N, Ohnishi Y. Genotyping the mouse severe combined immunodeficiency mutation using the polymerase chain reaction with confronting two-pair primers (PCR-CTPP). Exp Anim. 2002; 51:391–393. [PubMed: 12221933]

McCulley DJ, Kang JO, Martin JF, Black BL. BMP4 is required in the anterior heart field and its derivatives for endocardial cushion remodeling, outflow tract septation, and semilunar valve development. Dev Dyn. 2008; 237:3200–3209. [PubMed: 18924235]

Medici D, Kalluri R. Endothelial-mesenchymal transition and its contribution to the emergence of stem cell phenotype. Semin Cancer Biol. 2012

Medici D, Potenta S, Kalluri R. Transforming growth factor-beta2 promotes Snail-mediated endothelial-mesenchymal transition through convergence of Smad-dependent and Smad-independent signalling. The Biochemical journal. 2011; 437:515–520. [PubMed: 21585337]

Medici D, Shore EM, Lounev VY, Kaplan FS, Kalluri R, Olsen BR. Conversion of vascular endothelial cells into multipotent stem-like cells. Nat Med. 2010; 16:1400–1406. [PubMed: 21102460]

Nakashima K, Zhou X, Kunkel G, Zhang Z, Deng JM, Behringer RR, de Crombrugghe B. The novel zinc finger-containing transcription factor osterix is required for osteoblast differentiation and bone formation. Cell. 2002; 108:17–29. [PubMed: 11792318]

Okazaki M, Takeshita S, Kawai S, Kikuno R, Tsujimura A, Kudo A, Amann E. Molecular cloning and characterization of OB-cadherin, a new member of cadherin family expressed in osteoblasts. J Biol Chem. 1994; 269:12092–12098. [PubMed: 8163513]

Otsuru S, Tamai K, Yamazaki T, Yoshikawa H, Kaneda Y. Circulating bone marrow-derived osteoblast progenitor cells are recruited to the bone-forming site by the CXCR4/stromal cell-derived factor-1 pathway. Stem cells. 2008; 26:223–234. [PubMed: 17932420]

Romano LA, Runyan RB. Slug is an essential target of TGFbeta2 signaling in the developing chicken heart. Dev Biol. 2000; 223:91–102. [PubMed: 10864463]

Rossert J, Eberspaecher H, de Crombrugghe B. Separate cis-acting DNA elements of the mouse pro-alpha 1(I) collagen promoter direct expression of reporter genes to different type I collagen-producing cells in transgenic mice. J Cell Biol. 1995; 129:1421–1432. [PubMed: 7775585]

Roudier MP, Morrissey C, True LD, Higano CS, Vessella RL, Ott SM. Histopathological assessment of prostate cancer bone osteoblastic metastases. J Urol. 2008; 180:1154–1160. [PubMed: 18639279]

Sartor O, Coleman R, Nilsson S, Heinrich D, Helle SI, O'Sullivan JM, Fossa SD, Chodacki A, Wiechno P, Logue J, et al. Effect of radium-223 dichloride on symptomatic skeletal events in patients with castration-resistant prostate cancer and bone metastases: results from a phase 3, double-blind, randomised trial. The Lancet Oncology. 2014; 15:738–746. [PubMed: 24836273]

Sealey AL, Hobbs NK, Schmidt EE. Molecular genotyping of the mouse scid allele. J Immunol Methods. 2002; 260:303–304. [PubMed: 11792398]

Vakar-Lopez F, Cheng CJ, Kim J, Shi GG, Troncoso P, Tu SM, Yu-Lee LY, Lin SH. Up-regulation of MDA-BF-1, a secreted isoform of ErbB3, in metastatic prostate cancer cells and activated osteoblasts in bone marrow. J Pathol. 2004; 203:688–695. [PubMed: 15141384]

van Meeteren LA, ten Dijke P. Regulation of endothelial cell plasticity by TGF-beta. Cell Tissue Res. 2012; 347:177–186. [PubMed: 21866313]

Walter-Yohrling J, Morgenbesser S, Rouleau C, Bagley R, Callahan M, Weber W, Teicher BA. Murine endothelial cell lines as models of tumor endothelial cells. Clin Cancer Res. 2004; 10:2179–2189. [PubMed: 15041739]

Wu TT, Sikes RA, Cui Q, Thalmann GN, Kao C, Murphy CF, Yang H, Zhau HE, Balian G, Chung LW. Establishing human prostate cancer cell xenografts in bone: induction of osteoblastic reaction by prostate-specific antigen-producing tumors in athymic and SCID/bg mice using LNCaP and lineage-derived metastatic sublines. Int J Cancer. 1998; 77:887–894. [PubMed: 9714059]

Yeung F, Law WK, Yeh CH, Westendorf JJ, Zhang Y, Wang R, Kao C, Chung LW. Regulation of human osteocalcin promoter in hormone-independent human prostate cancer cells. J Biol Chem. 2002; 277:2468–2476. [PubMed: 11684680]

Yu PB, Deng DY, Lai CS, Hong CC, Cuny GD, Bouxsein ML, Hong DW, McManus PM, Katagiri T, Sachidanandan C, et al. BMP type I receptor inhibition reduces heterotopic ossification. Nat Med. 2008; 14:1363–1369. [PubMed: 19029982]

Zeisberg EM, Tarnavski O, Zeisberg M, Dorfman AL, McMullen JR, Gustafsson E, Chandraker A, Yuan X, Pu WT, Roberts AB, et al. Endothelial-to-mesenchymal transition contributes to cardiac fibrosis. Nat Med. 2007a; 13:952–961. [PubMed: 17660828]

Zeisberg EM, Tarnavski O, Zeisberg M, Dorfman AL, McMullen JR, Gustafsson E, Chandraker A, Yuan X, Pu WT, Roberts AB, et al. Endothelial-to-mesenchymal transition contributes to cardiac fibrosis. Nature medicine. 2007b; 13:952–961.

Zhou X, Zhang Z, Feng JQ, Dusevich VM, Sinha K, Zhang H, Darnay BG, de Crombrugghe B. Multiple functions of Osterix are required for bone growth and homeostasis in postnatal mice. Proceedings of the National Academy of Sciences of the United States of America. 2010; 107:12919–12924. [PubMed: 20615976]

Zhu F, Friedman MS, Luo W, Woolf P, Hankenson KD. The transcription factor osterix (SP7) regulates BMP6-induced human osteoblast differentiation. J Cell Physiol. 2012; 227:2677–2685. [PubMed: 21898406]

Highlights

- Osteoblasts in human PCa bone metastasis specimens co-express osteocalcin and Tie2
- Human prostate cancer bone metastases express high levels of BMP4
- BMP4 induces tumor-associated endothelial cells to become osteoblasts
- Deletion of *Osx* in endothelial cells in mice reduces PCa-induced bone formation

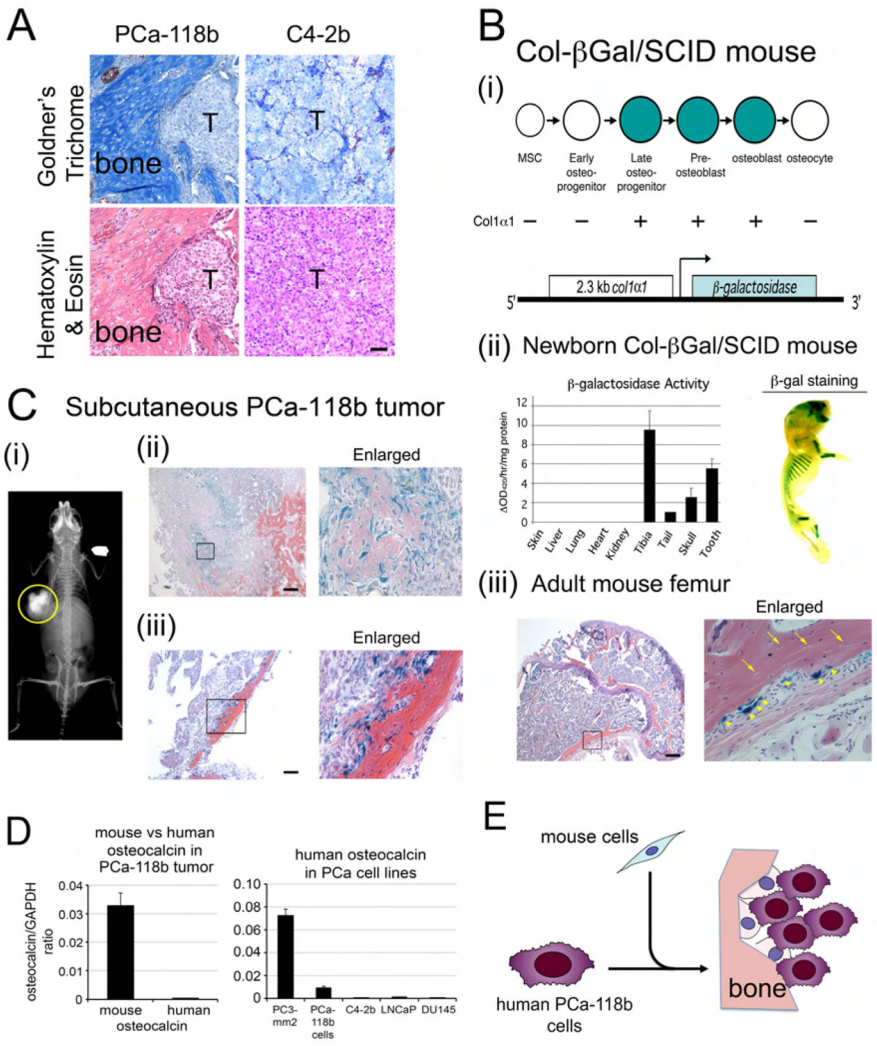

Figure 1. Ectopic bone in PCa-118b xenograft originates from the mouse host

(A) Consecutive sections of subcutaneous tumors generated from PCa-118b or C4-2b cells were stained with Goldner's Trichome or hematoxylin & eosin. T, tumor. Scale bar, 50 μm. (B) β-galactosidase expression in a *Col-βGal/SCID* mouse. (i) 2.3 kb *Col1α1*-driven *β-gal* construct in *Col-βGal/SCID* mouse. (ii) Left, β-galactosidase activity in lysates prepared from indicated tissues of a 4 day-old Col-βGal/SCID pup. Right, detection of β-galactosidase activity using X-gal as a substrate in the skull, rib, and hind limb of a 4 day-old *Col-βGal/SCID* mouse. (iii) X-gal staining of a femur from an adult *Col- βGal/SCID* mouse. Right, higher magnification of the boxed area on the left. Arrows, osteocytes; arrowheads, osteoblasts. Scale bar, 250 μm. (C) PCa-118b tumors in a *Col-βGal/SCID* mouse. (i) Radiograph of a calcified subcutaneous PCa-118b tumor (circled) in a *Col-βGal/SCID* mouse. (ii) X-gal staining of a PCa-118b tumor containing immature bone. Immature bone showed lighter eosin staining compared to the mature bone. (iii) X-gal staining of a PCa-118b tumor containing mature bone. Right, higher magnification of the boxed area on the left. Scale bar, 250 μm. (D) qRT-PCR for the expression of mouse or human osteocalcin from RNA prepared from PCa-118b whole tumor or isolated PCa-118b cells. (E) Diagram

illustrating the mouse origin of osteoblasts in the tumor-induced bone. Osteoblasts observed in PCa-118b xenograft are from mouse cells that are recruited into the tumor.

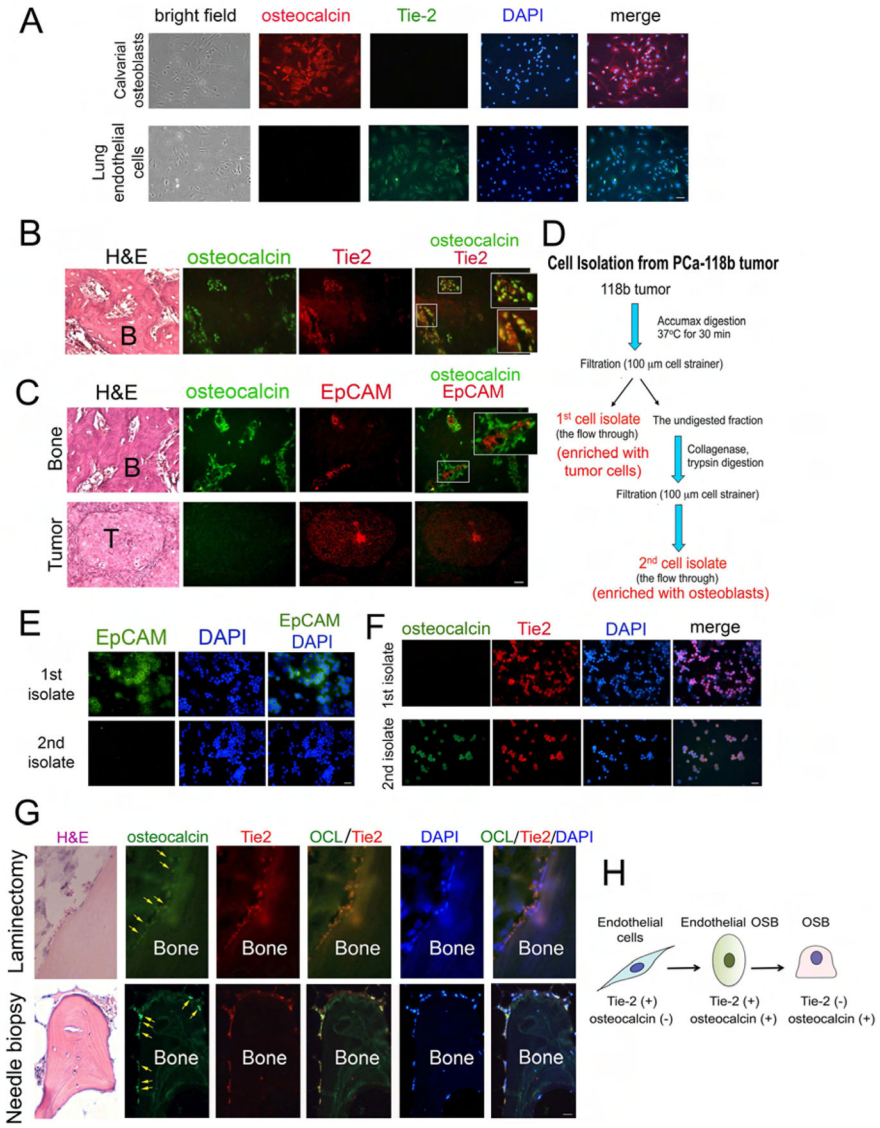

Figure 2. Osteoblasts in tumor-associated bone co-express endothelial cell and osteoblast markers

(A) Primary mouse osteoblasts isolated from 2–4 day old newborn calvaria were immunostained with antibodies against Tie2 and osteocalcin. Nuclei were stained with DAPI. Primary mouse osteoblasts expressed osteocalcin but not Tie2. In contrast, mouse endothelial cells expressed Tie2 but not osteocalcin. Scale bar, 50 μm(see also Figure S1). Representative sections of PCa-118b tumor co-stained with (B) osteocalcin and Tie-2 antibodies or (C) EpCAM and osteocalcin. Areas containing bone or tumor are shown. Boxed areas are enlarged in insets. B, bone; T, tumor. (D) Procedure for enrichment of different cell populations from a PCa-118b tumor. First cell isolate, tumor cell enriched population; second cell isolate, osteoblast enriched population. Immunostaining of first and second cell isolates with (E) antibody against EpCAM or (F) antibodies against Tie2 and osteocalcin (see also Figure S2A). (G) Immunostaining of osteocalcin (OCL) and Tie2 in human PCa bone metastasis specimens. Upper, a specimen from laminectomy. Lower, a

specimen from needle biopsy (see also Figures S3 and S4). (H) Diagram illustrating that some of tumor-associated endothelial cells are likely converted to osteoblasts based on the results from the expression of cell-specific markers. Scale bars, 25 μm.

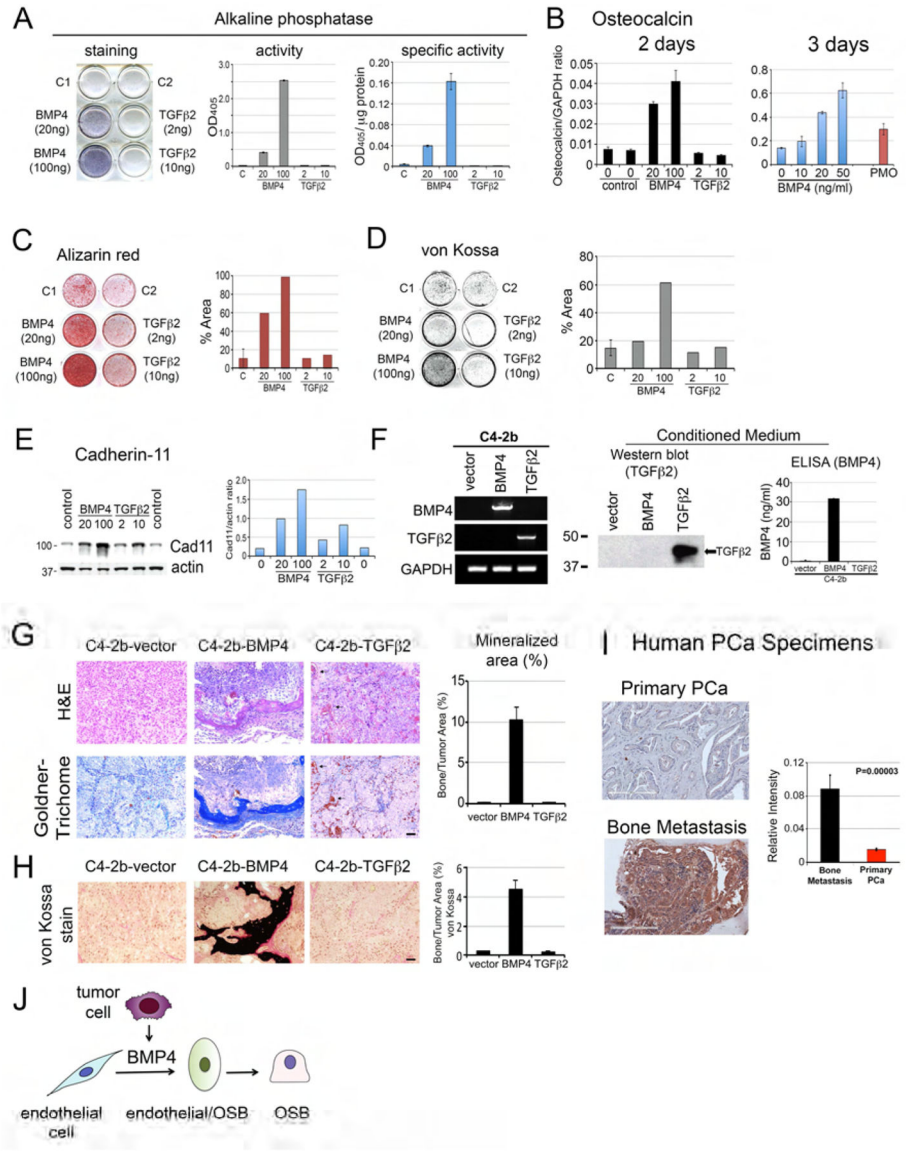

Figure 3. Effects of BMP4 or TGFβ2 on EC-to-OSB conversion in vitro and in vivo

(A) 2H11 endothelial cells were incubated in differentiation medium with indicated concentrations of BMP4 or TGFβ2 for 7 days. Left, the culture was stained with alkaline phosphatase substrate. Middle, cell lysates were incubated with p-nitrophenylphosphate and the OD_{405} measured. Right, alkaline phosphatase activity was normalized with the protein concentration. (B) qRT-PCR using primers for mouse osteocalcin on RNA from 2H11 cells treated with indicated concentrations of BMP4 or TGFβ2 for 2 or 3 days. The relative level of osteocalcin RNA induced in 2H11 cells was compared to that of mouse calvaria (PMO). (C) Alizarin Red S staining or (D) von Kossa staining of 2H11 cells in differentiation medium treated with BMP4 or TGFβ2 for 21 days. Right panels, quantification of the stainings using image J. (E) Western blot of 2H11 cell lysates prepared as in (B) using Cad11 or actin antibody. Right, quantification of Cad11 levels relative to actin. (F) Characterization of C4-2b-vector, C4-2b-BMP4, and C4-2b-TGFβ2 cells. Left, RT-PCR

using primers specific for BMP4 or TGFβ2. GAPDH message was used as a control. Middle, Western blot for the expression of TGFβ2 protein in the conditioned media. Right, ELISA for the expression of BMP4 in the conditioned media. (G) Histological analyses of C4-2b-vector, C4-2b-BMP4, and C4-2b-TGFβ2 tumors by H&E and Goldner's trichrome staining. Right, quantification of mineralized area in tumors based on Goldner's trichrome staining. Scale bars, 50 μm. (H) von Kossa staining of C4-2b-vector, C4-2b-BMP4, and C4-2b-TGFβ2 tumors and its quantification (right) in tumor sections. Scale bars, 50 μm. (I) Representative immunohistochemistry images of primary prostate cancer or bone biopsies stained for BMP4. Scale bar, 200 μm. Densitometry analyses of BMP4 expression in human prostate cancer specimens were quantified by Aperio ImageScope software. Data are presented as mean plus SEM. p value was determined by t-test. (J) Diagram illustrating that tumor secreted BMP4 is one of the factors produced by tumor cells that induce EC-to-OSB conversion to form ectopic bone.

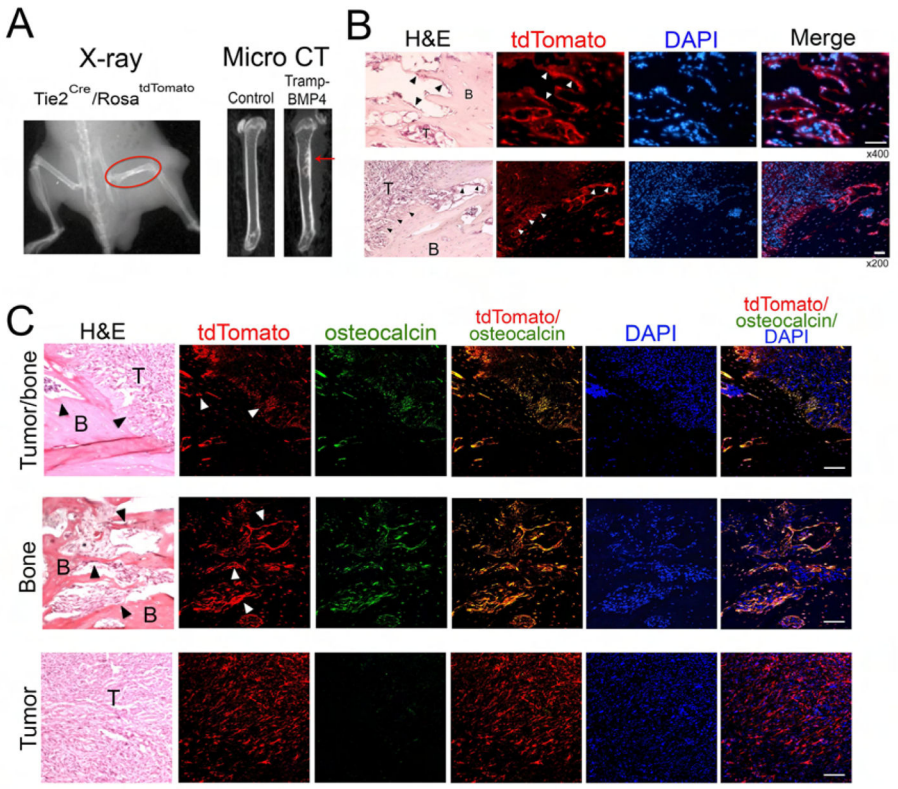

Figure 4. Co-localization of osteocalcin and tdTomato in osteoblasts of tumor-induced bone in $Tie2^{Cre}/Rosa^{tdTomato}$ mouse

In vivo lineage tracing of tumor-induced osteoblasts in $Tie2^{Cre}/Rosa^{tdTomato}$ mice. TRAMP-BMP4 cells (1 million) were injected into right femur of either Rosa-tdTomato or $Tie2^{Cre}/Rosa^{tdTomato}$ mice for seven weeks. Mice were subjected to radiograph analysis (A, left panel). Femurs were collected for micro CT (A, right panel). (B) Histological analyses. Scale bars are at 50 μm of x400 magnification (top panel) and at 50 μm of x200 magnification (bottom panel). (C) Immunostaining of osteocalcin. Confocal images of the co-expression of Tie2 (tdTomato) and osteocalcin (green). Scale bars are at 100 μm of x400 magnification. Arrowheads point to the tumor-induced osteoblasts.

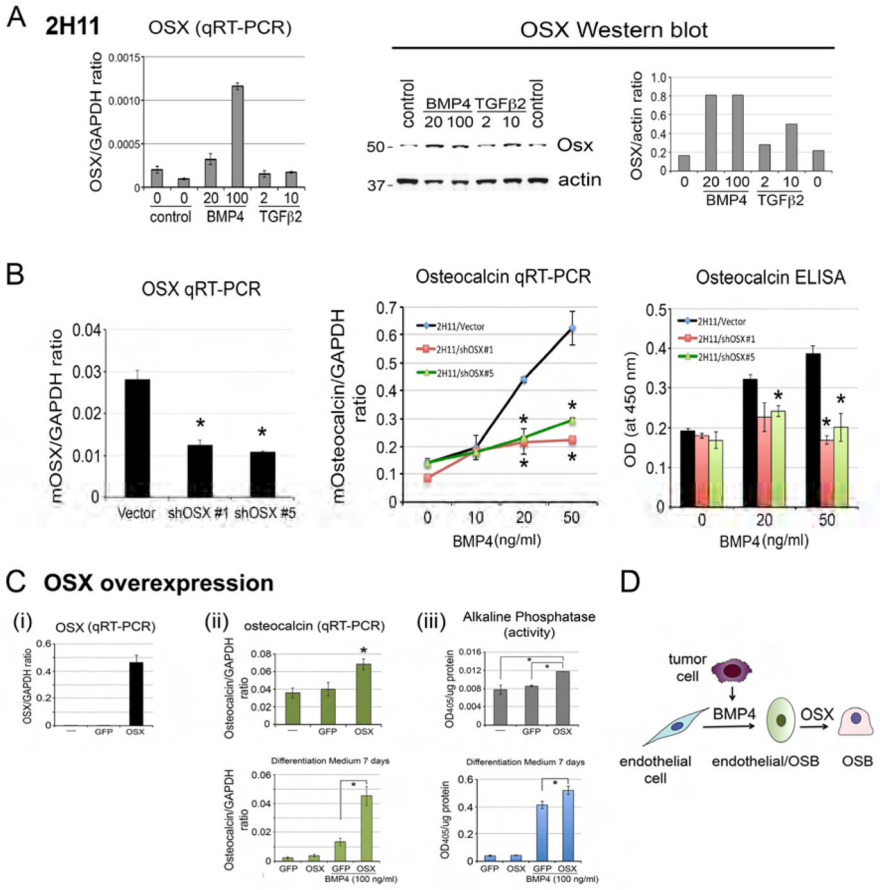

Figure 5. Role of OSX in EC-to-OSB conversion

(A) Left, qRT-PCR for the levels of *OSX* messages in BMP4 or TGFβ2-treated 2H11 cells. Right, western blot of lysates from BMP4 or TGFβ2-treated 2H11 cells with anti-OSX antibody. (B) qRT-PCR for OSX mRNA in 2H11-vector, 2H11-shOSX#1, and 2H11-shOSX#5 cells (left panel). When compared to 2H11-vector cells, osteocalcin expression induced by BMP4 was significantly reduced in 2H11-shOSX#1 and 2H11-shOSX#5 cells in mRNA (middle panel) and protein levels (right panel). (C) (i) qRT-PCR for OSX mRNA in 2H11, 2H11-GFP, and 2H11-OSX cells. (ii) Upper, qRT-PCR of osteocalcin mRNA upon incubation in differentiation medium with BMP4 for 7 days. Lower, Western blot of OSX protein in 2H11-GFP and 2H11-OSX cells cultured in differentiation medium with BMP4 for 7 days. (iii) Upper, alkaline phosphatase activity in 2H11, 2H11-GFP, and 2H11-OSX cells. Lower, alkaline phosphatase activity in 2H11-GFP and 2H11-OSX cells cultured in differentiation medium with BMP4 for 7 days. (D) Diagram illustrating that both BMP4 and OSX are necessary for EC-to-OSB conversion.

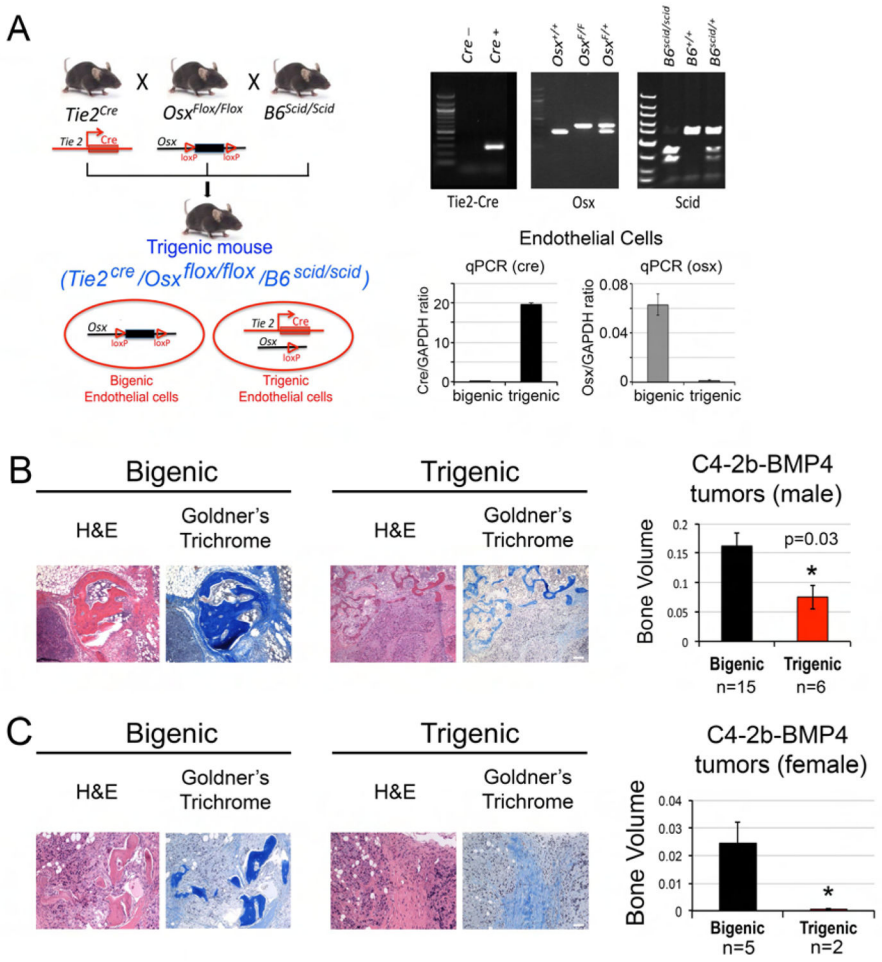

Figure 6. Tumor-induced ectopic bone in C4-2b-BMP4 tumors is significantly reduced in mice with endothelial-specific deletion of *OSX*

(A) Design and generation of bigenic $OSX^{f/f}/B6^{scid/scid}$ and endothelial-specific *OSX* knockout trigenic $Tie2^{cre}/OSX^{f/f}/B6^{scid/scid}$ mice. Upper right, mouse genotypes were determined by PCR. Lower right, qPCR for Cre or OSX in genomic DNA prepared from microvascular endothelial cells isolated from the lungs of bigenic and trigenic mice using CD31 magnetic beads. (B) H&E and Goldner's trichome staining of C4-2b-BMP4 tumors generated in male trigenic and bigenic mice. Right, quantification of ectopic bone in tumors. Scale bars, 100 μm. (C) C4-2b-BMP4 tumors generated in female trigenic and bigenic mice. Right, quantification of ectopic bone in tumors. n, number of tumor samples in each group. Scale bars, 50 μm.

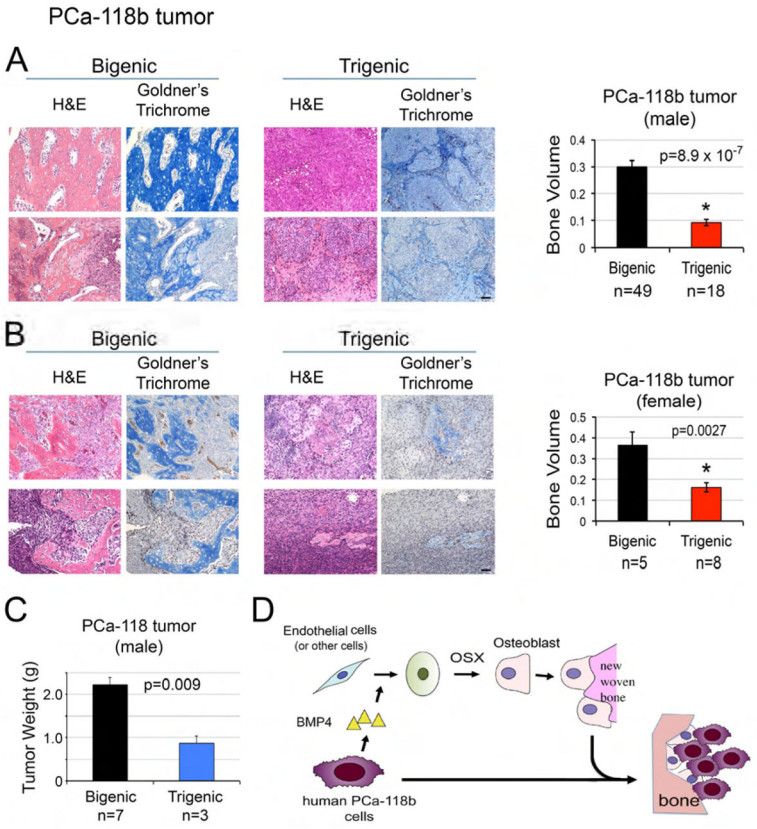

Figure 7. Tumor-induced ectopic bone in PCa-118b tumors is significantly reduced in mice with endothelial-specific deletion of OSX

(A) H&E and Goldner's trichome staining of PCa-118b tumor generated in male bigenic *OSX*$^{f/f}$/*B6*$^{scid/scid}$ and trigenic *Tie2*^{cre}/*OSX*$^{f/f}$/*B6*$^{scid/scid}$ mice described in Fig. 5A. Right, quantification of ectopic bone in tumors in males. n, number of tumor samples. (B) H&E and Goldner's trichome staining of PCa-118b tumor generated in female bigenic and trigenic mice. Right, quantification of ectopic bone in tumors in females. n, number of tumor samples in each group. (C) Quantification of tumor weight of PCa-118b tumors in male bigenic and trigenic mice. (D) Model of PCa-induced bone formation through endothelial-to-osteoblast conversion. PCa cells secrete factors, e.g. BMP4, which induce *OSX* expression in endothelial cells (or other stromal cells), leading to EC-to-OSB conversion. The EC-to-OSB conversion is one mechanism accounting for the characteristic osteoblastic bone lesion of PCa. Scale bars, 50 μm.